HHS Public Access

Author manuscript

Neuropharmacology. Author manuscript; available in PMC 2015 May 07.

Published in final edited form as:

Neuropharmacology. 2010 June ; 58(7): 972–980. doi:10.1016/j.neuropharm.2009.12.017.

Blood brain barrier permeability and tPA-mediated neurotoxicity

Taher Nassar[1], **Sergey Yarovoi**[2], **Anwar Rayan**[3], **Itschak Lamensdorf**[4], **Michael Karakoveski**[5], **Polianski Vadim**[5], **Rami Abu Fanne**[1], **Mahmud Jamal**[1], **Douglas B. Cines**[2], and **Abd Al-Roof Higazi**[1,2]

[1]Department of Clinical Biochemistry, Hebrew University - Hadassah Medical Center, Jerusalem, Israel

[2]Department of Pathology and Laboratory Medicine, University of Pennsylvania, Philadelphia, PA, USA

[3]QRC-Qasemi Research Center, Baka El-Garbiah, Israel

[4]Thrombotech Ltd, Ness Ziona, Israel.

[5]PharmaSeed Ltd, Ness Ziona, Israel.

Abstract

Tissue type plasminogen activator (tPA) induces neuronal apoptosis, disrupt the blood-brain-barrier (BBB), and promotes dilation of the cerebral vasculature. The timing, sequence and contributions of these and other deleterious effects of tPA and their contribution to post-ischemic brain damage after stroke, have not been fully elucidated. To dissociate the effects of tPA on BBB permeability, cerebral vasodilation and protease-dependent pathways, we developed several tPA mutants and PAI-1 derived peptides constructed by computerized homology modeling of tPA. Our data show that intravenous administration of human tPA to rats increases BBB permeability through a non-catalytic process, which is associated with reversible neurotoxicity, brain damage, edema, mortality and contributes significantly to its brief therapeutic window. Furthermore, our data show that inhibiting the effect of tPA on BBB function without affecting its catalytic activity, improves outcome and significantly extends its therapeutic window in mechanical as well as thromboembolic models of stroke.

Correspondence should be addressed to: Abd Al-Roof Higazi, M.D., Department of Pathology and Laboratory Medicine University of Pennsylvania 513A Stellar-Chance 422 Curie Boulevard Philadelphia, PA 19104 (p) 215-662-3966 (fax) 215-673-2012 higazi@mail.med.upenn.edu.

Contributions: A.A.H. designed the research; T.N., S.Y., A.R., M.K., P.V., R.A.F., and M.J. performed the research and collected data; A.A.H., I.L., and D.B.C analyzed the data; A.A.H., and D.B.C. wrote the paper.

Disclosures: I.L. works at Thrombotech Ltd and M.K., and P.V., work at PharmaSeed Ltd[5], Ness Ziona, Israel.

Introduction

Endogenous and exogenous tPA have the potential to aggravate ischemic brain damage after vascular occlusion(Nagai et al. 1999; Wang et al. 1998) or traumatic brain injury (TBI)(Mori et al. 2001) by increasing infarct size and cerebral edema. The mechanism by which tPA causes these neurotoxic effects has not been fully elucidated. tPA promotes the activation of metalloproteases that lead to matrix degradation and disrupts the blood-brain-barrier (BBB) (Yepes et al. 2003). tPA also activates glutamate receptors, which mobilize intracellular calcium and mediate apoptosis of cortical cells(Choi 1988; Nicole et al. 2001), and augments dilation of the cerebral vasculature in non-ischemic areas, thereby decreasing blood flow to the penumbra(Armstead et al. 2006; Nassar et al. 2004). The specific contribution of each of these components to the neurotoxicity of tPA is not clear since in most experimental models many of these pathways are activated concurrently. The primary goal of this study is to elucidate the molecular bases of tPA mediated opening of the BBB and its contribution to post-ischemic brain damage.

Brain parenchyma is exposed to tPA released from endogenous sources after injury(Armstead et al. 2005; Yepes 2000) and from exogenous sources when tPA is used to treat ischemic stroke. The importance of this distinction is highlighted by recent findings that intraventricular, but not intravenous (IV), administration of catalytically active murine tPA increases BBB permeability in mice(Su et al. 2008). This finding helps to explain the deleterious effect of endogenous tPA in stroke(Wang et al. 1998) and TBI(Mori et al. 2001). It also suggests that the neurotoxicity of recombinant tPA (rtPA) given IV to treat stroke may not derive primarily from its ability to further enhance BBB permeability. Identifying the mechanism by which tPA permeabilizes the BBB will not only increase our understanding of the mechanism neurotoxicity but might point to ways to mitigate neurological injury.

We have previously reported that tPA initiates intracellular signaling in vascular cells through receptor mediated processes that are independent of its catalytic activity(Armstead et al. 2005; Nassar et al. 2004). Signaling is inhibited by a hexapeptide derived from plasminogen activator inhibitor 1 (PAI-1). The peptide interacts with the PAI-1 docking site in tPA, which lies outside of its catalytic center and therefore does not affect its capacity to activate its physiological substrate plasminogen to inhibit fibrinolysis(Armstead et al. 2006; Nassar et al. 2004). This peptide provides neuroprotection against endogenous as will exogenous tPA in models of stroke and TBI(Armstead et al. 2006), data that has been recently reproduced by others(Tan et al. 2009).

If tPA permeabilizes the BBB from within the CNS through a process dependent on its catalytic activity(Yepes et al. 2003), it would be difficult to envision how this deleterious effect could be vitiated without compromising its fibrinolytic activity. On other hand, these observations were made with recombinant mouse tPA(Yepes et al. 2003), which differs from human tPA within the PAI-1 docking (human “aa 295-99” AKHRR; mouse VKNKR), which is essential for intracellular signaling(Armstead et al. 2006; Nassar et al. 2004). This suggests that effect of intravenous human tPA on BBB function may differ.

To pursue this possibility, we used human recombinant tPA to elucidate the molecular bases of BBB permeability and its contribution to post-ischemic brain damage. We tested the hypothesis that intravenous human tPA may increase BBB permeability through non-catalytic processes, which would afford the opportunity to inhibit this receptor mediated process without compromising fibrinolytic (catalytic) activity. Our findings suggest a novel approach to preserving BBB function that improves the outcome of stroke in animals treated with tPA and increases its therapeutic window.

Materials and Methods

PAI-1 derived peptides

Peptides were synthesized as previously described by Peptisyntha (Brussels, Belgium and San Diego, CA). *rtPA:* (Actilase) was purchased from Boehringer (Ingelheim, Germany). *Catalytically inactive rtPA (tPAS^{481}A)*: cDNA encoding mouse wild type (WT-tPA) and tPA-S^{481}A were expressed in Drosophila S2 cells and purified using antibody-affinity chromatography. The proteins migrate as single bands at Mr ~55 kDa on SDS-PAGE and their plasminogen activator activity was analyzed using the plasmin chromogenic substrate SpectrazymePL (gift of American Diagnostica), as described(Higazi et al. 1995).

Anesthesia—All experimental protocols involving the use of vertebrate animals were approved by the Israeli Board for Animal Experiments. Sprague-Dawley rats (Harlan Laboratories, Jerusalem, Israel) were anesthetized with an intraperitoneal injection of ketamine (75 mg/ml) and xylazine (5 mg/ml) Kepro, Holland) prior to study.

Transient occlusion of the middle cerebral artery—Transient occlusion of the middle cerebral artery (MCA) was performed exactly as described previously(Armstead et al. 2006). Briefly, the left common carotid artery (CCA) was exposed and permanently ligated. An incision was made in the CCA to insert a 4-0 monofilament nylon suture. The monofilament was inserted through the CCA into the lumen of the ICA. The monofilament was advanced into the circle of Willis, effectively occluding the middle carotid artery (MCA). Two to four hours after MCA occlusion, the monofilament was removed.

Thromboembolic Stroke—Focal ischemia was induced by injecting microemboli as described(Armstead et al. 2006). Donor rats were anesthetized as above and their femoral arteries were catheterized. Arterial blood (0.1 ml) was obtained and incubated at room temperature for 2 hours to induce clot formation. The clot was fragmented by passage through a 26-gauge needle. Recipient rats were anesthetized with 1.5% isoflurane to maintain spontaneous respiration. The bifurcations of the right CCA, ICA and ECA were exposed. The occipital artery branches of the ECA were then isolated. The ICA was isolated and from the adjacent vagus nerve, and the pterygopalatine artery was ligated close to its origin. Next, a 4-0 silk suture was tied loosely around the mobilized ECA stump, and a PE-50 polyethylene tube was connected to a 21-guide needle, positioned within the ECA to a location 1 or 2 mm distal to the bifurcation of the CCA and then fixed. The microclots were injected gently into the ICA over a period of 10 seconds. The PE-50 tube was removed and the ECA ligated. Rectal temperatures were maintained at 37°C with a heating lamp.

Treatment—Treatments were administered by intravenous (IV) infusion. After the induction of the ischemic or thrombotic stroke, animals were randomly divided into several cohorts (n = 12-16 animals per group as indicated in figure legends). Animals in each cohort were injected with either: 1) saline 2) saline containing rtPA (6 mg/kg), or 3) saline containing rtPA together PAI-1 derived peptide 6-aa or 18-aa Tyr (1 mg/kg each) or 4) 6-aa or 18-aa Tyr peptides alone. Fifty percent of the dose was given as a bolus injection and the remainder was infused over 60 min. Tubes containing each form of treatment were coded and handed to the surgeon who was blinded to nature of the intervention. Statistical analysis was performed by a third party who was also blinded to the experimental conditions.

Neuro-score assessment—Two assessments of neurological function (neuro-scores, NSS) were performed 24 hours post induction of ischemia on a total of 12 and 18 animals, respectively, as described(Chen et al. 2001).

Assessment of BBB integrity—BBB permeability was measured using Evans blue(Adelson et al. 1998) or radiolabeled fibrinogen as described(Higazi et al. 1998). Anesthetized rats were injected IV with 100 μl of saline or saline containing either WT-rtPA or catalytically inactive rtPA-Ser^{481}Ala (1 mg/kg each) alone or together PAI-1 or the PA-1 derived peptides (1 mg/kg). Five minutes later, the rats were given an IV injection of 2% Evans blue (EB) or radiolabeled fibrinogen (0.5 mg/kg) in saline. One hour after this second injection, organs were cleared of blood by transcardiac perfusion. The brains were removed, weighed, homogenized in N,Ndimethylformamide and centrifuged. Extruded dye was quantified by absorbance at 620 nm or by quantifying radioactivity, as described(Higazi et al. 1998). Data are expressed as absorbance or cpm per gram of tissue.

Plasminogen activator activity—Plasminogen activator activity was determined as previously reported(Higazi et al. 2005) by adding WT tPA, WT uPA or PA variants(20 nM each) to a reaction mixture containing Glu–plasminogen (100 nM) and the plasmin chromogenic substrate Spectrazyme PL (500 μM) in phosphate-buffered saline (PBS) at 37°C. The light absorbance at 405 nm was measured continuously over time. The initial velocity of plasmin generation was calculated from the change in the rate of A_{405} over different time intervals and the results were expressed as the change in optical density (ΔOD) per minute.

Assessment of infarction and hemorrhage—. Twenty-four hours after induction of stroke, rats were euthanized using CO_2. The brains were rapidly removed and sectioned coronally into 2 mm segments. All slices were examined under a surgical microscope to evaluate for hemorrhagic transformation. The slices were then incubated in 2% 2,3,5-triphenyltetrazolium chloride (TTC) solution for 30 minutes at 37°C and fixed overnight at room temperature in 4% buffered formaldehyde solution (Gadot, Haifa, Israel). Each TTC-stained brain slice was then photographed with a digital camera (Olympus C-4000, Japan).

Measurement of Infarct Size—The infarcted area in each section was measured using an image J analysis system. The total infarct volume was determined by integrating the areas from all sections and the results were expressed as a percentage of the total volume of the ipsilateral hemisphere, as described(Tejima et al. 2001).

Mortality—The animals were included in the study once treatment had been initiated. Death was recorded only in treated animals.

Modeling of tPA—The resolution coordinates of the serine protease domain at 3.25 Å, ID code 1PDA(Renatus et al. 1995) defined by X-ray, and the coordinates of the kringle-2 domain, ID code 1PK2(Byeon and Llinás 1991) defined by NMR, were downloaded from the Protein Data Bank(Abola et al. 1997) and used to model the 3D structure of tPA. The dynamics simulation module in Discovery Studio 2.0 was used for molecular dynamics (MD) simulations. All calculations were made using a dual Intel Pentium IV 3.0 GHz processor.

The initial structure was built through the following steps: 1. Assembly of serine protease with kringle-2: Cys-Ser-Thr-Cys segment was found in more than 50 PDBs. Their coordinates were extracted and used to build dozens of optional models. Hydrogens were added and charges were assigned in $p^H = 7.0$. Structures were minimized by fixing the main chain coordinates except the two residues (Ser and Thr) from the connecting loop with 1000 steps of steep descent and 5000 steps of conjugate gradients. 2. Homology modeling of Kringle-1: the sequence identity between kringle-1 and kringle-2 is 53%. 1PK2 (the NMR structure of kringle-2) was used as a template for homology modeling of kringle-1 in Discovery Studio 2.0. Restraints for backbone atoms of identical residues (kringle-1/ kringle-2) were applied. One thousand steps of steep descent and five thousand of conjugate gradient minimization were performed at first for hydrogens followed by side chains and later for the whole model of kringle-1. 3. Assembly with kringle-1: the lowest energy structure obtained previously was used to connect with the lowest energy model of kringle-1.

The time step of 1 fs was used to integrate the equations of motion. The structure was minimized by fixing the main chain coordinates of the whole protein with the exception of the two connecting loops with 1000 steps of steep descent and 5000 steps of conjugate gradients. The structure was heated to 1000 K and run for 1 ns of production simulation at constant pressure (1 atm). The structure was then minimized with the combination of 1000 steps of steep descent and 5000 steps of conjugate gradients. This was repeated 100 times, generating 100 frames. The lowest energy structure obtained by MD (see Figure 1) was used for docking. This model shows good stereochemistry, as assessed by PROCHECK(Laskowski 2003). Residues from the two predicted connecting loops lie in the allowed region of the Ramachandran plot. The all-atom contact analysis with MOLPROBITY(Davis et al. 2007) shows no clashes inside the model.

Molecular Docking—Docking was carried out by using Autodock 4.0(Morris et al. 1998). The AutoDockTools package (AutoDockTools was downloaded from the website http://autodock.scripps.edu/downloads/resources/adt/. The starting structures for docking of the two peptides, the shorter one composed of 6 amino acids (EEIIMD) and the longer one composed of 18 amino acids (RMAPEEIIMDRPFLFVVR) were extracted from the 2.6 Å resolution coordinates of PAI-1, ID code 1C5G(Tucker et al. 1995). The default protocol was applied and one hundred docked structures were generated using genetic algorithm searches. Docking poses with RMSD less than 1.0 Å were clustered together, represented by

the pose with the lowest free energy of binding. Complexes were minimized with 1000 steps of steepest descent followed by 5000 steps of conjugate gradients using Discovery Studio 2.0 while fixing the main chain of the protein structure, with the exception of the two connecting loops (kringle1-kringle2, kringle-2-serine protease).

Statistical analysis—All data are presented as mean ± SE. Differences were analyzed by the t-test and the level of significance was corrected using post-hoc analysis with the Bonferroni test. One way ANOVA with Newman Keuls post-hoc test was also used as indicated in the text for in between group analysis as described(Nassar et al. 2007). Statistical significance was set at $P < 0.05$.

Results

Involvement of the catalytic activity of tPA in BBB permeability

To elucidate the molecular basis of tPA mediated opening of the BBB, we began by examining the requirement for expression of catalytic activity. To address this question, we used a human rtPA variant (tPA-Ser^{481}Ala) that lacks catalytic activity. A single IV injection of 1 mg/kg the tPA-Ser^{481}Ala variant to unmanipulated rats increased BBB permeability, as measured by extravasation of Evans blue (Figure 1A). The effect of tPA-Ser^{481}Ala was similar to that of WT-rtPA (Figure 1A). This finding mitigates against a requirement for the catalytic activity of intravenously administered exogenous human rtPA to disrupt the BBB and suggests that permeabilization may be mediated through a signal transduction process as in the case of tPA's effect on vascular contractility(Akkawi et al. 2006; Armstead et al. 2006; Nassar et al. 2004).

To study the putative non-catalytic signal transduction pathway of rtPA-mediated BBB permeability in greater detail, we examined the effect of the PAI-1 derived hexapeptide Ac-EEIIMD-amide. Ac-EEIIMD-amide inhibits both tPA-induced signal transduction in vascular smooth muscle cells(Akkawi et al. 2006) and its effect on cerebral vasodilation(Nassar et al. 2004), and decreases neuronal death and infarct size in several models of brain injury(Armstead et al. 2006) without affecting its catalytic activity. However, Ac-EEIIMD-amide did not inhibit rtPA-mediated BBB permeability (Figure 1A).

Ac-EEIIMD-amide was developed in order to mimic the neuroprotective effect of PAI-1 observed in PAI$^{-/-}$ mice (i.e. increased in infarct size compared to WT mice) in a stroke model caused by mechanical occlusion of the MCA(Nagai et al. 1999), without inhibiting the salutary effects of rtPA on thrombolysis(Nassar et al. 2004). The failure of Ac-EEIIMD-amide to inhibit rtPA-induced BBB permeability was therefore not expected, but could mean that mechanisms involved in barrier disruption differ from those involved in its extra-catalytic activities (e.g. cerebral vasodilation) and that the effect of tPA on BBB permeability is independent of PAI-1. Alternatively, Ac-EEIIMD-amide may not fully recapitulate the extracatalytic activities of PAI-1. To distinguish between these possibilities, we examined the effect of PAI-1 on rtPA-mediated opening of the BBB. Equimolar concentrations of PAI-1 completely inhibited the increased BBB permeability induced by rtPA (Figure 1A). This is consistent with the concept that Ac-EEIIMD-amide provides

incomplete protection against the non-catalytic activities of rtPA because it lacks a critical portion of the PAI-1 molecule.

Effect of extended PAI-1 derived peptides on BBB permeability

Ac-EEIIMD-amide comprises a portion of PAI-1 that binds to rtPA at a site outside the catalytic triad(Madison et al. 1990a; Madison et al. 1989; Madison et al. 1990b). Based on the inhibitory effect of PAI-1, we tested the hypothesis that PAI-1 differs from Ac-EEIIMD-amide in the extent to which it binds to the docking site of rtPA and thereby modulates its three dimensional structure and extracatalytic activity.

Therefore, our next step was to identify the minimal effective fragment of PAI-1 that inhibits rtPA-mediated disruption of BBB integrity without affecting its catalytic activity by examining various PAI-1 derived peptides that retain the core Ac-EEIIMD-amide sequence but contain progressively longer flanking sequences derived from native PAI-1. We found that the sequence Ac-RMAPEEIIMDR-amide inhibited rtPA-induced BBB permeability to a greater extent than Ac-EEIIMD-amide ($P < 0.002$) (Figure 1B). Increasing the length of the PAI-1 derived peptide on the carboxylic side further enhanced its inhibitory activity. Thus, the 18-aa peptide (Ac-RMAPEEIIMDRPFLFVVR-amide) proved to be more effective than the 11-aa peptide (Ac-RMAPEEIIMDR-amide) ($P < 0.009$) (Figure 1B), inhibiting rtPA-induced BBB permeability by more than 80% (Figure 1B). A 18-aa peptide in which the 6 amino acid core peptide was scrambled (Ac-RMAPDMIIEERPFLFVVR-amide) was devoid of inhibitory activity (Figure 1B). The 11-aa and 18-aa peptides, like their EEIIMD core, but not the scrambled peptide, also inhibited vasodilation (Figure 2A) without affecting the catalytic activity of rtPA (Figure 2B).

To further support our findings, we studied the effect of tPA on the exudation of radiolabeled fibrinogen from the blood into the brain parenchyma as an independent means to measure BBB permeability and its regulation by tPA and PAI-1 derived peptides. Fibrinogen was chosen because it deposits in brain tissue in neuropathological conditions as Alzheimers disease and is a well-described marked of BBB permeability(Alafuzoff et al. 1987; Chen et al. 2008; Ryu and McLarnon 2009; Sabel et al. 2003). rtPA increased the exudation of radiolabeled fibrinogen from the blood into the CNS parenchyma (Figure 2C). Permeation was inhibited by PAI-1 and the 18-aa PAI-1 derived peptide, but not by the 6-aa or scrambled peptide, concordant with the effect on extravasation of Evans blue (Figure 1B).

Interaction of extended PAI-1 derived peptides with rtPA

To begin to understand the basis of the differences in binding of the various PAI-1 derived peptides to rtPA, we constructed a model of the enzyme by homology modeling and studied molecular interactions with the PAI-1 derived peptides via simulated docking experiments. The potential interactions between the three PAI-1 derived peptides with the tPA molecule are shown in Figure 3. Each peptide preferentially interacts with tPA in its linear form at the previously identified PAI-1 docking site close to the active site of the molecule.

This model also predicts that the 18-aa peptide interacts with several residues in tPA in addition to those that form contacts with the 6-aa and 11-aa peptides. Based on these simulations, Ac-EEIIMD-amide contains 3 residues that are predicted to interact with rtPA:

E^{373} has an electrostatic interaction with K^{296} in tPA, while I^{375} and M^{377} interact through hydrophobic bonds with V^{343} and P^{345} in tPA, respectively. In contrast, the 18-aa peptide has 7 residues (R^{369}, M^{370}, E^{373}, I^{375}, M^{377}, L^{382}, V^{384}) that are projected to have strong interactions with tPA and 5 others (P^{380}, F^{381}, F^{383}, V^{385}, R^{386}) that interact partially with the enzyme. It is worth noting that the 3 residues that mediate the binding of the 6-aa peptide to rtPA (E^{373}, I^{375} and M^{377}) also participate in the binding of the 18-aa peptide and that 9 of the residues added to the 6-aa to generate the 18-aa peptide on each side of the core 6-aa peptide (Ac-RMAPEEIIMDRPFLFVVR-amide) also participate in binding.

To assess the validity of the model, we compared the capacity of the 6-aa and 18-aa peptides to compete with the binding of PAI-1 to rtPA. The EC_{50} of the 18-aa peptide was approximately 3-fold lower than that of the 6-aa peptide (Figure 4A), supporting the contention that the binding of the longer peptide simulates the binding of PAI-1 more closely than does EEIIMD.

Enhancing the bioavailability of the 18-aa peptide

The 18-aa peptide is relatively insoluble in an aqueous environment. The lyophilized peptide required resuspension in 50% ethanol at 37°C and it had to be vortexed for maximal solubility (0.2 mg/ml). This limitation has the potential to compromise its bioavailability and efficacy at high concentrations (Figure 4A).

We attributed the limited solubility of the original 18-aa peptide to the prevalence of hydrophobic amino acid residues on the carboxy-terminal side of the elongated peptide (PFLFVV). Therefore, we modified the composition of the 18-aa peptide to enhance its solubility in aqueous solutions, a process that would facilitate attempts to maximize dosing *in vitro* and *in vivo* and improve its delivery to ischemic tissue. We chose to enhance solubility by substituting a hydrophilic amino acid based on the model that predicts the aromatic ring of Phe^{383} is directed outward toward the solvent (Figure 4B). We reasoned that substituting Tyr for Phe at this position would maintain the aromatic ring but improve solubility by adding a hydroxyl group without affecting significantly its interaction with tPA. As predicted, Ac-RMAPEEIIMDRPFLYVVR-amide was more soluble in an aqueous environment than the original sequence; specifically, at room temperature, 18-aa-Tyr^{383} is soluble in 50% ethanol at concentrations up to 5 mg/ml, with no additional steps required. Substitution of Tyr^{383} for Phe^{383} improved the capacity of the 18-aa peptide to compete with the binding of PA-1 to rtPA, reducing the EC_{50} from 272 nM to 42 nM (Figure 4A) and its capacity to inhibit rtPA-induced BBB permeability was similar to that of PAI-1 itself (data not shown). Moreover, the original 18-aa- Phe^{383} and the mutated 18-aa-Tyr^{383} peptides, like their 6-aa core (EEIIMD), inhibited rtPA-induced vasodilation without inhibiting the catalytic activity of rtPA. Therefore, we studied the *in vivo* activity of 18-aa-Tyr^{383} in two models of stroke.

Effect of PAI-1 derived peptides and BBB permeability on neurological sequelae of ischemic stroke

Studied together, the 6-aa, 18-aa wild-type and 18-aa-Tyr^{383} peptides can be used to dissociate the effect of tPA on BBB permeability from its effect on cerebral vasodilation.

This enabled us to evaluate the role of BBB disruption in accentuating post-ischemic brain damage induced by rtPA. In order to examine this question, we compared the effect of 6-aa and 18-aa-Tyr^{383} peptides on neurological recovery in rats treated with rtPA after induction of stroke by mechanical occlusion of the MCA (tMAO).

Injection of rtPA (6 mg/kg) one hour after the initiation of MCA occlusion and withdrawal of the filament increased infarct size by approximately 56% ($P < 0.0007$) (Figure 5A). At this time, the increase in infarct size was almost entirely prevented ($P < 0.001$) in animals that had been given either the 6-aa or 18-aa-Tyr^{383} peptide together with rtPA (Figure 5A). By two hours after withdrawal of the filament, animals injected with rtPA alone showed an increase in infarct size of approximately 62% ($P < 0.024$) (Figure 5B). At this time point, infarct size was significantly smaller in animals given the 18-aa-Tyr^{383} peptide together with rtPA compared with those receiving the 6-aa peptide with rtPA ($P < 0.004$) or rtPA alone. By three hours after reperfusion, only 18-aa-Tyr^{383} maintained its capacity to inhibit the extension of infarct size in rtPA-treated animals (Figures 5C and 5D).

Administration of rtPA three hours after withdrawal of the filament resulted in increased mortality (Figure 6A) and aggravated the neurological disability, as reflected in the neurological severity score (NSS) (Figure 6B). Co-injection of 18-aa-Tyr^{383}, but not the 6-aa peptide, decreased the mortality associated with rtPA from 28.6±4.2% to 15.4±2.9% ($P < 0.05$) (Figure 6A). Furthermore, 18-aa-Tyr^{383} significantly ($P < 0.04$) improved the NSS in animals given rtPA compared with animals treated with rtPA alone (Figure 6B). Thus, there was a close correlation between the effect of rtPA and the PAI-1 derived peptides on infarct volume and the improvement in neurological function in all settings tested.

We then tested the hypothesis that the prolonged neuroprotection provided by 18-aa-Tyr^{383} stems from its capacity to neutralize the disruption of BBB permeability by rtPA. To address this question, we analyzed the relationship between the time course of BBB permeabilization after tMCAO and loss of neuroprotection by the 6-aa peptide. The time course of BBB permeability post tMCAO is shown in Figure 7. Permeability was maximal one hour after withdrawal of the filament. Barrier integrity was significantly ($P < 0.007$), but not totally, restored by three hours. Administration of rtPA three hours after the filament was withdrawn re-opened the BBB. This late effect of rtPA on BBB permeability was almost completely (96.7%) inhibited by 18-aa-Tyr^{383} but not by the 6-aa peptide (Figure 7).

Effect of extending the duration of BBB integrity on neurological sequelae

Lastly, we addressed the implications of extending the duration of BBB integrity. To do so, we asked whether blocking rtPA-mediated BBB permeability would extend its therapeutic window in a thromboembolic model of stroke (MCAO) in which the net beneficial effect of rtPA stemming from its fibrinolytic activity is evaluated in the context of its deleterious effects. Three hours after embolic stroke was established, administration of rtPA together with 18-aa-Tyr^{383}, but not with the 6-aa peptide, improved the outcome compared with animals treated with rtPA alone, as evidenced by a reduction in stroke volume (Figures 8A and B) and preservation of neurological function (Figure 8C). Furthermore, co-injection of rtPA and 18-aa-Tyr^{383} three hours after embolic stroke reduced rtPA-induced mortality and

ICH by 66.7% and 53.64%, respectively, compared with animals treated with rtPA alone ($P < 0.05$ for each).

Discussion

The data presented in this paper support the contention that the neurotoxicity of tPA is multifactorial and time-dependent. The 6-aa PAI-1 derived peptide antagonist that inhibits rtPA-induced cerebral vasodilation without affecting BBB permeability, reduces infarct size at one hour but not at 3 hours after brain ischemia induced by mechanical occlusion of the MCA. This finding indicates that cerebral vasoactivity plays an important role in the deleterious effect of rtPA during the first hour after the onset of cerebral ischemia. Over the ensuing several hours, the activity of the 6-aa peptide is not sufficient to reduce infarct size or to preserve motor function, suggesting that other mechanisms are operative and dominant by this time.

Three hours after induction of brain ischemia by mechanical vascular occlusion, the BBB remains disrupted in animals treated with rtPA. The 6-aa peptide fails to block this effect, limit infarct size or preserve motor function, whereas the 18-aa peptide that blocks rtPA induced BBB permeabilization in addition to preventing cerebral vasodilation, is neuroprotective at both time points. This finding suggests that permeabilization of the BBB contributes to the delayed and protracted neurotoxicity of rtPA and that approaches that inhibit its effect on BBB permeability may extend its therapeutic window. This concept is supported by the results using the peptide 18-aa-Try in a thromboembolic model of stroke. The benefit seen three hours post brain ischemia in animals that had been given 18-aa-Tyr may reflect a combined effect of mitigating the loss of BBB integrity and inhibiting specific signal transduction mechanisms, such as preventing untoward vasodilation(Armstead et al. 2006).

Our data together with those of Su et al(Su et al. 2008), suggest that tPA and rtPA-mediated permeabilization of the BBB is species specific. Mouse tPA appears to disrupt the BBB only from within the CNS, whereas human rtPA induces BBB permeabilization when its is given intravenously as well. Moreover, induction of BBB permeability by mouse, but not human rtPA, requires catalytic activity(Su et al. 2008). The fortuitous finding that the effect of human rtPA on BBB integrity and cerebral vasodilation does not require its catalytic activity and the difference in amino acid composition of the region responsible for this signal-transduction effect(Armstead et al. 2006), provide an opportunity to develop agents that isolate its beneficial effect on fibrinolysis, prolong its therapeutic window and have the potential to improve the management of patients with stroke.

Acknowledgments

Funding Sources: This work was supported by Grants HLHL077760, NS53410, HD5735501 and HL076406 from the National Institutes of Health and 930/04 from the Israel Science Foundation.

Literature

Abola EE, Sussman JL, Prilusky J, Manning NO. Protein Data Bank archives of three-dimensional macromolecular structures. Methods Enzymol. 1997; 227:556–571. [PubMed: 9379928]

Adelson PF, Whalen MJ, Kochanek PM. Blood brain barrier permeability and acute inflammation in two models of traumatic brain injury in the immature rat: a preliminary report. Acta Neurochir Suppl. 1998; 71:104–106. al. e. [PubMed: 9779157]

Akkawi S, Nassar T, Tarshis M, Cines BC, Higazi AA-R. LRP and avB3 mediate tPA-activation of smooth muscle cells. Am J Physiol Heart Circ Physiol. 2006; 291:H1351–1359. [PubMed: 16489109]

Alafuzoff I, Adolfsson R, Grundke-Iqbal I, Winblad B. Blood-brain barrier in Alzheimer dementia and in non-demented elderly. An immunocytochemical study. Acta Neuropathol. 1987; 73:160–166. [PubMed: 3300132]

Armstead W, Cines D, Higazi AA-R. Plasminogen activators contribute to age dependent impairment of NMDA cerebrovasodilation after brain injury. Develop Brain Res. 2005; 156:139–146.

Armstead W,M, Nassar T, Akkawi S, Smith D,H, Chen X,H, Cines D,B, Higazi AA-R. Neutralizing the neurotoxic effects of exogenous and endogenous tPA. Nat Neurosci. 2006; 9:1150–1155. [PubMed: 16936723]

Byeon IJ, Llinás M. Solution structure of the tissue-type plasminogen activator kringle 2 domain complexed to 6-aminohexanoic acid an antifibrinolytic drug. J Mol Biol. 1991; 222:1035–1051. [PubMed: 1762144]

Chen J, Sanberg PR, Li Y, Wang L, Lu M, Willing AE, Sanchez-Ramos J, Chopp M. Intravenous Administration of Human Umbilical Cord Blood Reduces Behavioral Deficits After Stroke in Rats. Stroke. 2001; 32:2682–2688. [PubMed: 11692034]

Chen X, Gawryluk J, Wagener J, Ghribi O, Geiger J. Caffeine blocks disruption of blood brain barrier in a rabbit model of Alzheimer's disease. J Neuroinflammation. 2008; 5:12. PMID: 18387175. [PubMed: 18387175]

Choi D. Glutamate toxicity and diseases of the nervous system. Neuron. 1988; 1:623–634. [PubMed: 2908446]

Davis IW, Leaver-Fay A, Chen VB, Block JN, Kapral GJ, Wang X, Murray LW, Arendall WB, Snoeyink J, Richardson JS, Richardson DC. MolProbity: all-atom contacts and structure validation for proteins and nucleic acids. Nucleic Acids Res. 2007; 35:W375–383. [PubMed: 17452350]

Haj-Yejia A, Nassar T, Sachais BS, Kuo A, Bdeir K, Al-Mehdi AB, Mazar A, Cines DB, Higazi AA-R. Urokinase-derived peptides regular vascular smooth muscle cell contraction in vitro and in vivo. FASEB J. 2000; 14:1411–1422. [PubMed: 10877834]

Higazi AA-R, Ajawi F, Akkawi S, Hess E, Kuo A, Cines BC. Regulation of the single-chain urokinase–urokinase receptor complex activity by plasminogen and fibrin: novel mechanism of fibrin specificity. Blood. 2005; 105:1021–1028. [PubMed: 15353482]

Higazi AA-R, Barghouti II, Abu-Much R. Identification of an inhibitor of tissue-type plasminogen activator-mediated fibrinolysis in human neutrophils. J Biol Chem. 1995; 270:9472–9477. [PubMed: 7721874]

Higazi AA-R, Bdeir K, Hiss E, Arad S, Kuo A, Barghouti I, Cines DB. Lysis of plasma clots by urokinase-soluble urokinase receptor complexes. Blood. 1998; 92:2075–2083. [PubMed: 9731065]

Laskowski RA. Structural quality assurance. Methods Biochem Anal. 2003; 44:273–303. [PubMed: 12647391]

Madison E, Goldsmith E, Gething M, Sambrook J, Gerard R. Restoration of serine protease-inhibitor interaction by protein engineering. J. Biol. Chem. 1990a; 265:21423–21426. [PubMed: 2123870]

Madison EL, Goldsmith EJ, Gerard R, Gething MJ, Sambrook J. Serpin-resistant mutants of human tissue-type plasminogen activator. Nature. 1989; 339:721–725. [PubMed: 2500599]

Madison EL, Goldsmith EJ, Gerard RD, Gething MJH, Sambrook JF, Bassel-Duby RS. Amino acid residues that affect interaction of tissue plasminogen activator with plasminogen activator inhibitor 1. Proc Natl Acad Sci U S A. 1990b; 87:3530–3534. [PubMed: 2110366]

Mori T, Wang X, Kline AE, Siao CJ, Dixon CE, Tsirka SE, Lo EH. Reduced cortical injury and edema in tissue plasminogen activator knockout mice after brain trauma. Neuroreport. 2001; 12:4117–4120. [PubMed: 11742249]

Morris GM, Goodsell DS, Halliday RS, Huey H, Hart WE, Belew RK, Olson JA. Automated docking using a Lamarckian genetic algorithm and an empirical binding free energy function. J. Comput. Chem. 1998; 19:1639–1662.

Nagai N, De Mol M, Lijnen HR, Carmeliet P, Collen D. Role of plasminogen system components in focal cerebral ischemic infarction. Circulation. 1999; 99:2440–2444. [PubMed: 10318667]

Nassar H, Lavi E, Akkawi S, Bdeir K, Heyman N,S, Raghunath O,N, Tomaszewski J, Higazi AA-R. Alpha-Defensin: Link between inflammation and atherosclerosis. Atherosclerosis. 2007; 194:452–457. [PubMed: 16989837]

Nassar T, Akkawi S, Shina A, Haj-Yehia A, Bdeir K, Tarshis M, Heyman S, Higazi AA-R. The in vitro and in vivo effect of tPA and PAI-1 on blood vessel tone. Blood. 2004; 103:897–902. [PubMed: 14512309]

Nicole O, Docagne F, Ali C, Margaill I, Carmeliet P, MacKenzie ET, Vivien D, Buisson A. The proteolytic activity of tissue-plasminogen activator enhances NMDA receptor-mediated signaling. Nat Med. 2001; 7:59–64. [PubMed: 11135617]

Renatus M, Engh RA, Stubbs MT, Huber R, Fischer S, Kohnert U, Bode W. Lysine 156 promotes the anomalous proenzyme activity of tPA: X-ray crystal structure of single-chain human tPA. EMBO J. 1995; 16:4797–4805. [PubMed: 9305622]

Ryu J, McLarnon J. A leaky blood-brain barrier, fibrinogen infiltration and microglial reactivity in inflamed Alzheimer's disease brain. J Cell Mol Med. PMID. 2009:18657226.

Sabel M, Rommel F, Kondakci M, Gorol M, Willers R, Bilzer T. Locoregional opening of the rodent blood-brain barrier for paclitaxel using Nd:YAG laser-induced thermo therapy: a new concept of adjuvant glioma therapy? Lasers Surg Med. 2003; 33:75–80. [PubMed: 12913878]

Su JE, Fredriksson L, Geyer M, Folestad E, Cale J, Andrae J, Gao Y, Pietras K, Mann K, Yepes M, Strickland KD, Betsholtz C, Eriksson U, Lawrence AD. Activation of PDGF-CC by tissue plasminogen activator impairs blood-brain barrier integrity during ischemic stroke. Nat Med. 2008; 14:731–737. [PubMed: 18568034]

Tan Z, Li X, Kelly K, Rosen C, Huber J. Plasminogen activator inhibitor type 1 derived peptide, EEIIMD, diminishes cortical infarct but fails to improve neurological function in aged rats following middle cerebral artery occlusion. Brain Res. 2009; 1281:84–90. [PubMed: 19465008]

Tejima E, Katayama Y, Suzuki Y, Kano T, E.H. L. Hemorrhagic transformation after fibrinolysis with tissue plasminogen activator: evaluation of role of hypertension with rat thromboembolic stroke model. Stroke. 2001; 32:1336–1340. [PubMed: 11387496]

Tucker HM, Mottonen J, Goldsmith EJ, Gerard RD. Engineering of plasminogen activator inhibitor-1 to reduce the rate of latency transition. Nat Struct Biol. 1995; 2:442–445. [PubMed: 7664104]

Wang Y, Tsirka S, Strickland S, Stieg P, Soriano S, Lipton S. Tissue plasminogen activator (tPA) increases neuronal damage after focal cerebral ischemia in wild-type and tPA-deficient mice. Nat Med. 1998; 4:228–231. [PubMed: 9461198]

Yepes M. Neuroserpin reduces cerebral infarct volume and protects neurons from ischemia-induced apoptosis. Blood. 2000; 96:569–576. [PubMed: 10887120]

Yepes M, Sandkvist M, Moore EG, Bugge TH, Strickland DS, Lawrence DA. Tissue-type plasminogen activator induces opening of the blood-brain barrier via the LDL receptor–related protein. J. Clin. Invest. 2003; 112:1533–1540. [PubMed: 14617754]

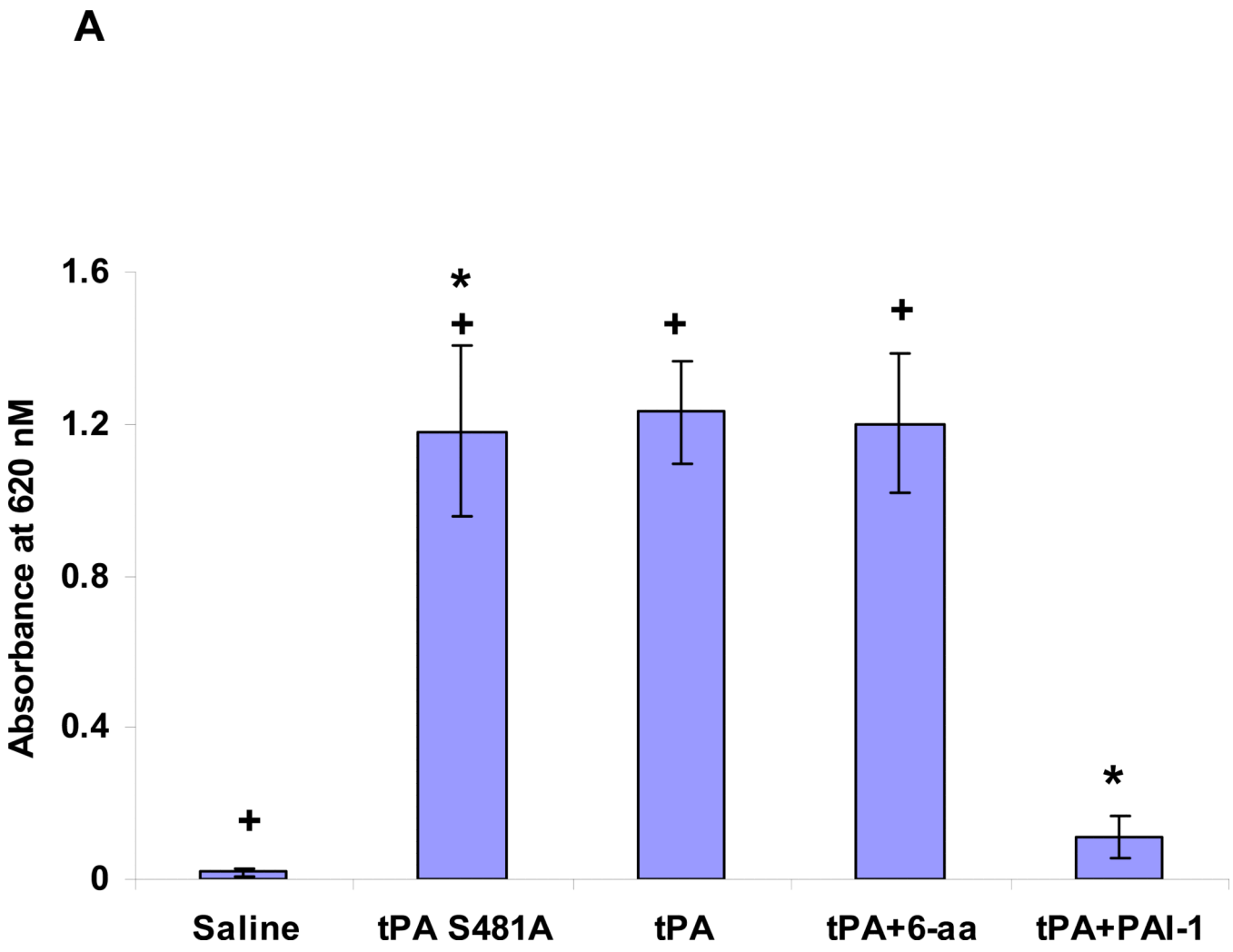

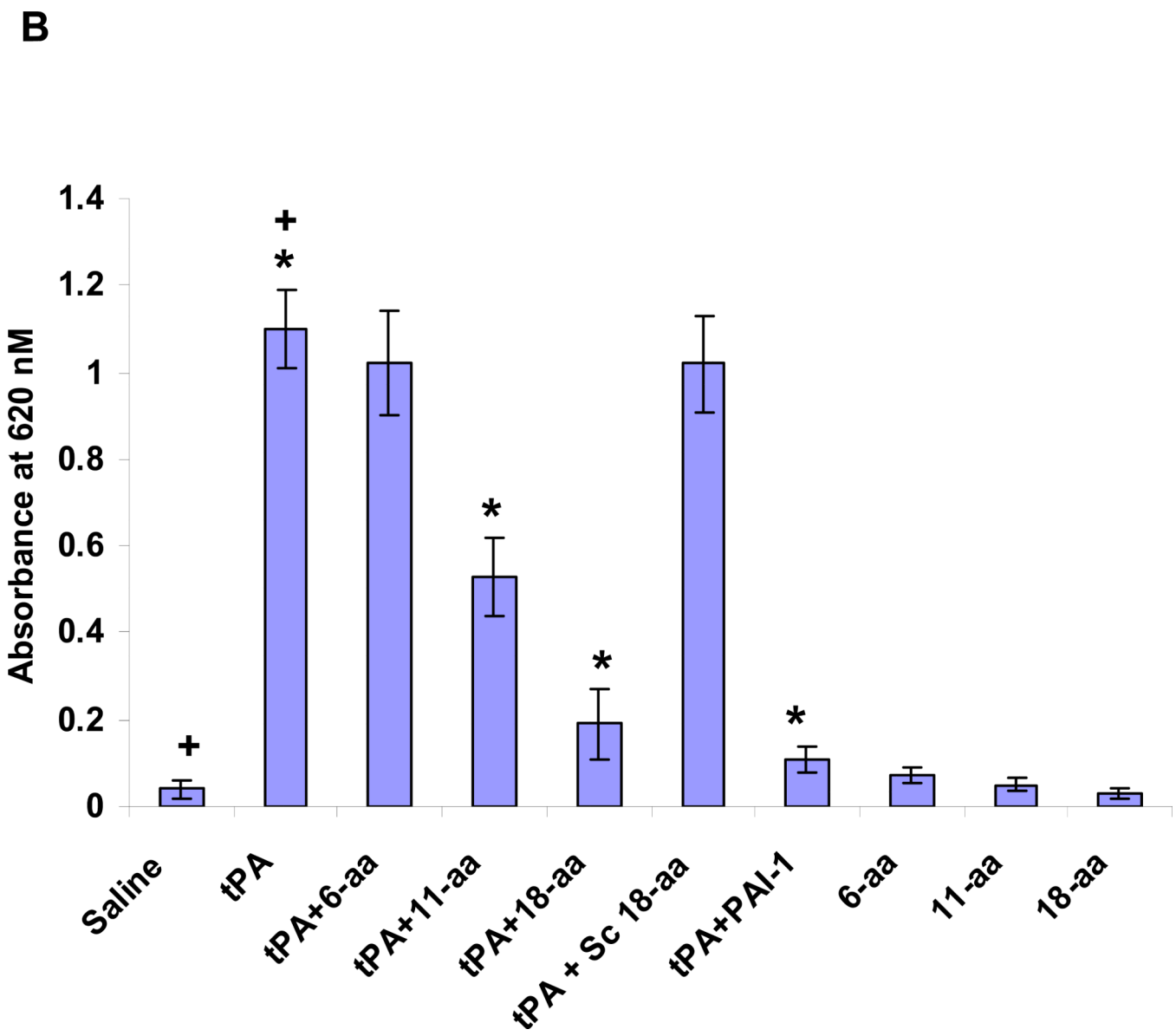

Figure 1. Regulation of BBB integrity by human rtPA and PAI-1. Panel A. Role of the catalytic activity of rtPA in BBB permeability

BBB permeability was measured using Evans blue(Adelson et al. 1998). Anesthetized rats were injected IV with 100 μl of saline or saline containing either WT-rtPA or catalytically inactive rtPA-Ser^{481}Ala (1 mg/kg each) alone or together with PAI-1 or the PA-1 derived peptide Ac-EEIIMD-amide (1 mg/kg). Five minutes later, the rats were given an IV injection of 2% Evans blue (EB) in saline. One hour after injection of the dye, organs were cleared of blood by transcardiac perfusion. The brains were removed, weighed, homogenized in N,N dimethylformamide and centrifuged. Extruded dye was quantified by absorbance at 620 nm. Data are expressed as absorbance per gram of tissue. The mean ± SEM of data from 6 animals/group is shown. Panel B. Effect of PAI-1 derived peptides on rtPA-induced BBB permeability. Three PAI-1 derived peptides of varying length derived from the core sequence EEIIMD, as described in the text (6-aa, 11-aa or 18-aa) were

injected alone (1mg/kg) or together with rtPA (1 mg/kg). Permeability was measured as described in the legend to Panel A. The mean ± SEM of data from 8-9 animals/group is shown. Statistical significance was set at $P < 0.05$ using t-test (+) or ANOVA test(*) in this and in each Figure that follows.

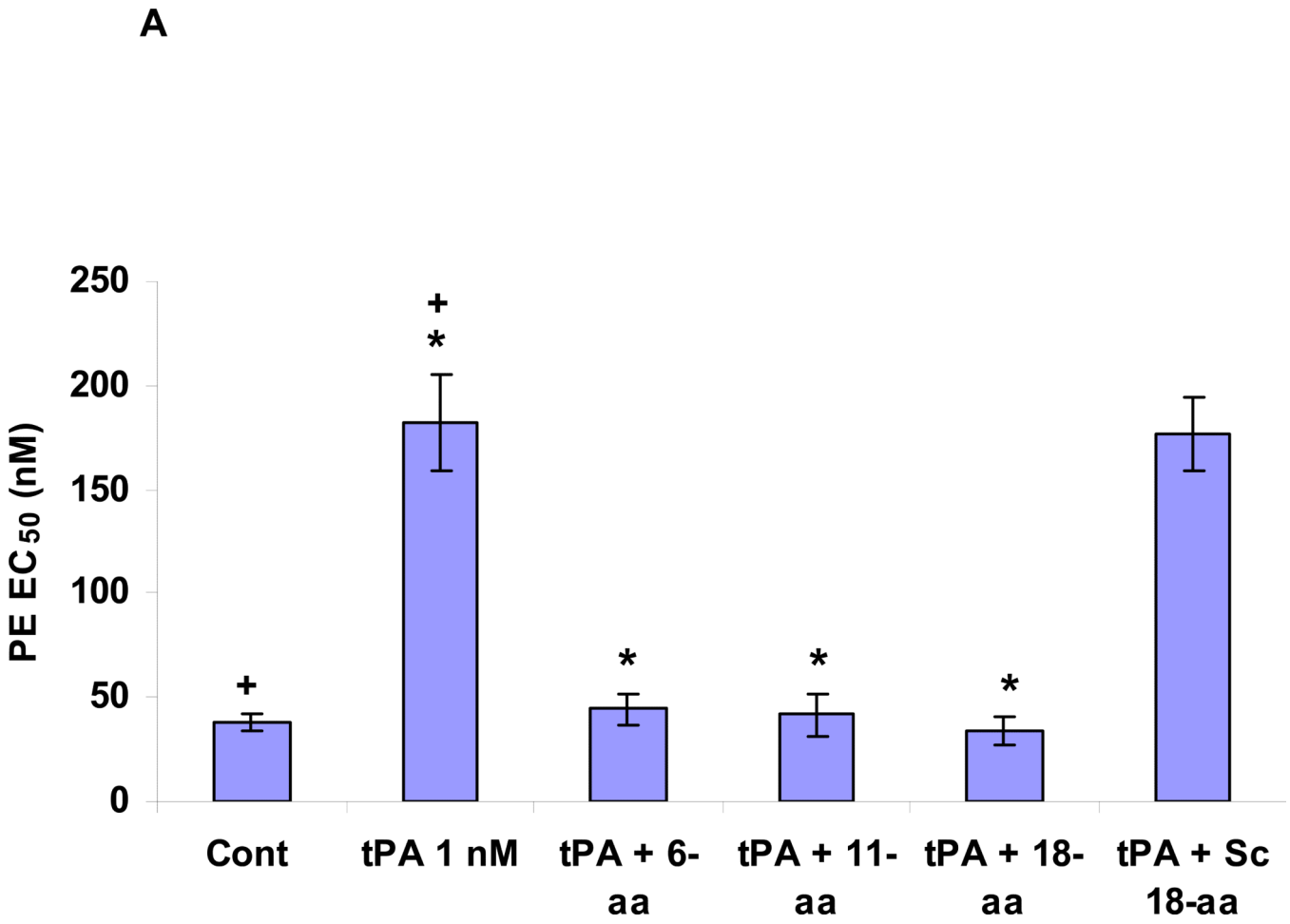

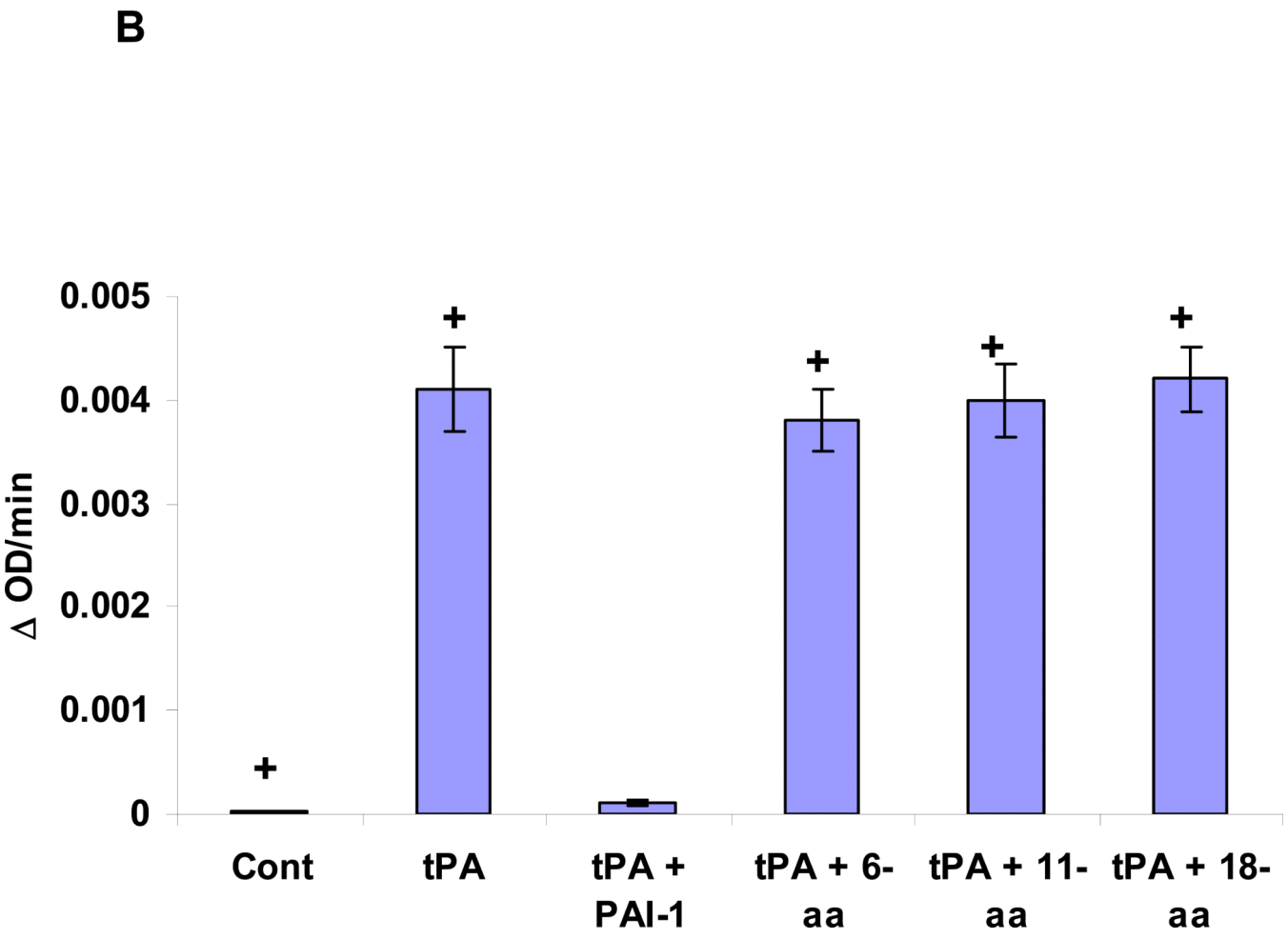

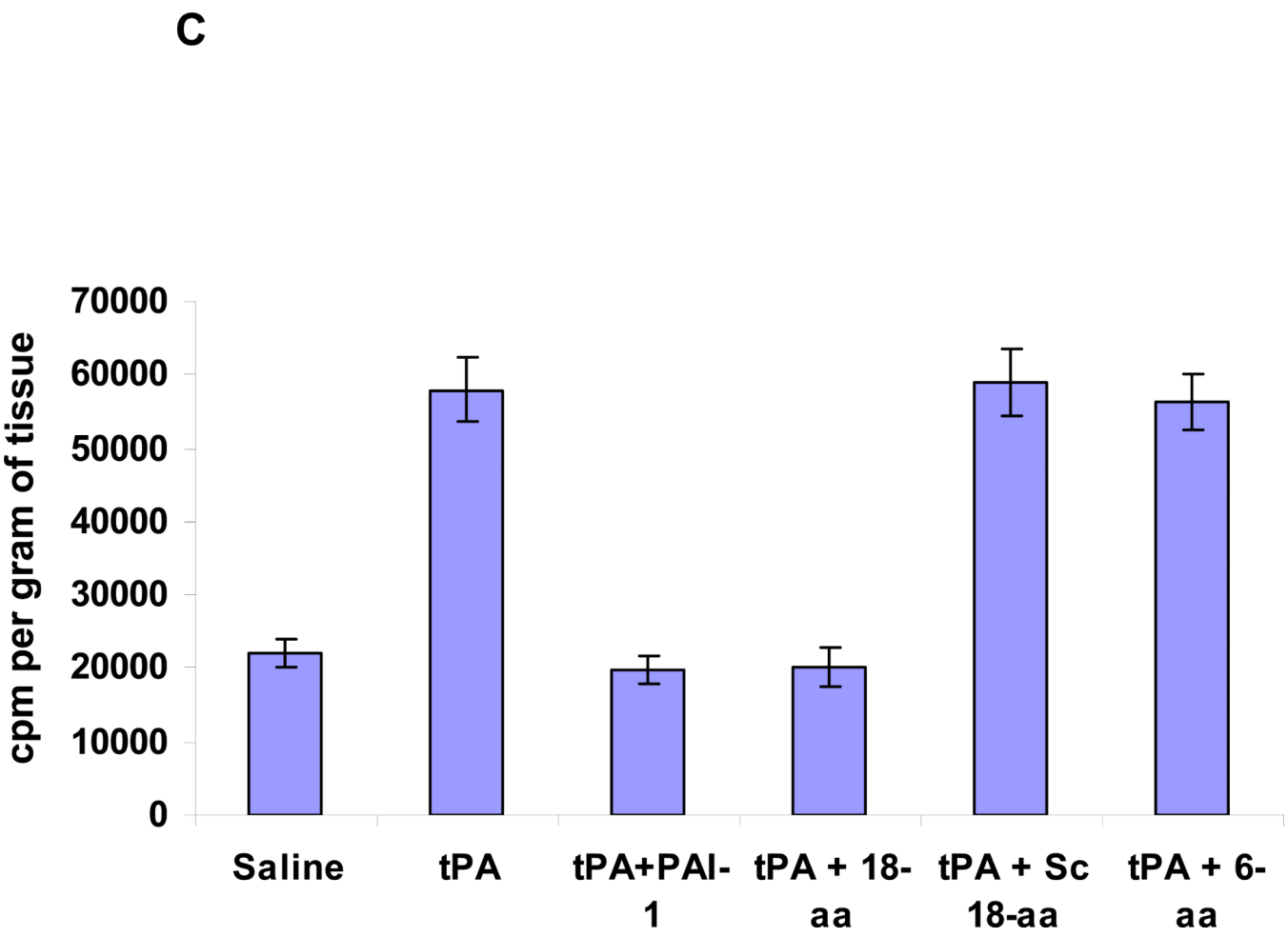

Figure 2. Panel A. Effect of PAI-1 derived peptides on tPA induced vasodilation

Contraction of isolated aortic rings was induced by adding increasing concentrations of phenylephrine (PE), as described in(Haj-Yejia et al. 2000; Nassar et al. 2004). The EC_{50} was determined in the absence or presence of rtPA (1 nM) alone or in the presence of the 6 (6-aa), 11 (11-aa), 18-aa (18-aa) PAI-1 derived peptide or the 18-aa scrambled (18-aa Sc) peptide (100 nM each). The mean ± SEM of data from 3 experiments is shown. Panel B. Effect of PAI-1 derived peptides on tPA induced plasminogen activation. The capacity of tPA to activate plasminogen was tested in absence or presence of PAI-1 or the PAI-1 derived peptides 6 (6-aa), 11 (11-aa), 18-aa (18-aa) or the 18-aa scrambled (18-aa Sc) peptide. The mean ± SD of data from 3 experiments is shown. Panel C. Effect of rtPA and PAI-1 derived peptides on extravasation of radiolabeled fibrinogen. Anesthetized rats were injected IV with 100 μl of saline or saline containing either WT-rtPA (1 mg/kg each) alone or together with PAI-1 or the PA-1 derived peptide Ac-EEIIMD-amide (1 mg/kg), 18-aa Tyr or scrambled 18-aa peptide. Five minutes later, the rats were given an IV injection of ^{125}I-labled fibrinogen (0.5 mg/ml, specific activity of 300,000 cpm/mL) in saline. One hour after injection of the ^{125}I-fibrinogen, organs were cleared of blood by transcardiac perfusion. The brains were removed, weighed and homogenized in N,N dimethylformamide. Radioactivity was quantified Using γ-counter. Data are expressed as cpm per gram of tissue. The mean ± SEM of data from 6 animals/group is shown.

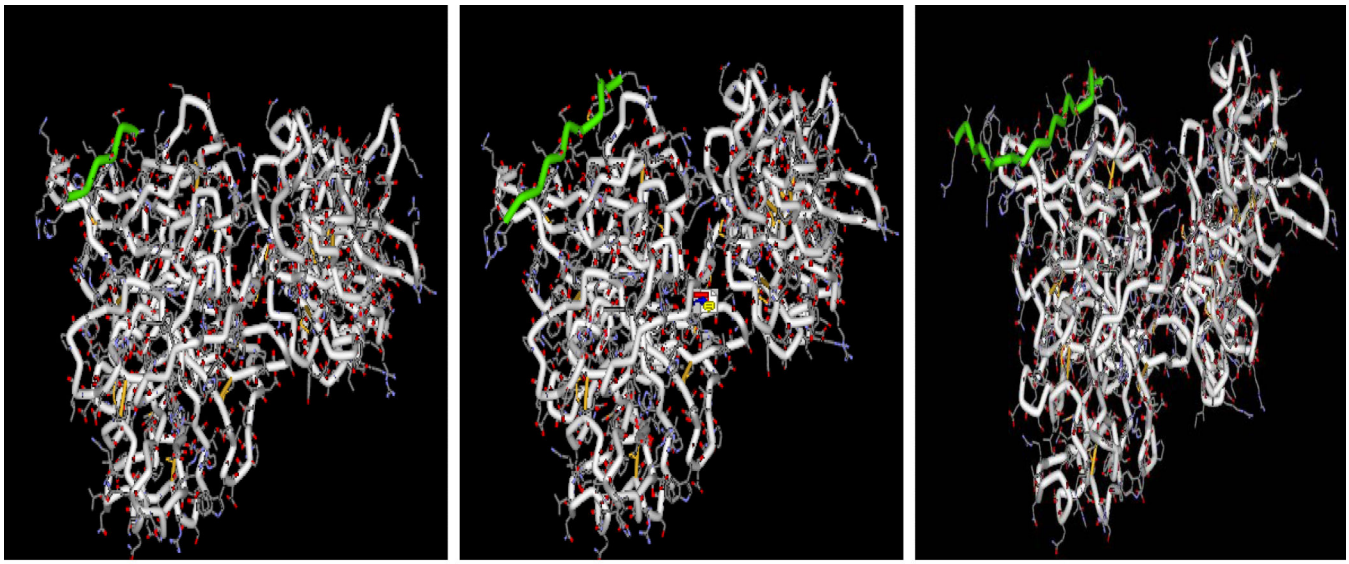

Figure 3. Representation of energetically favorable rtPA/PAI-1 derived peptide-peptide complexes

The peptides adopt an extended conformation upon binding to the previously described PAI-docking site in tPA. Most of the hydrophobic residues of the 18-aa peptide are buried within the hydrophobic surface regions of the enzyme.

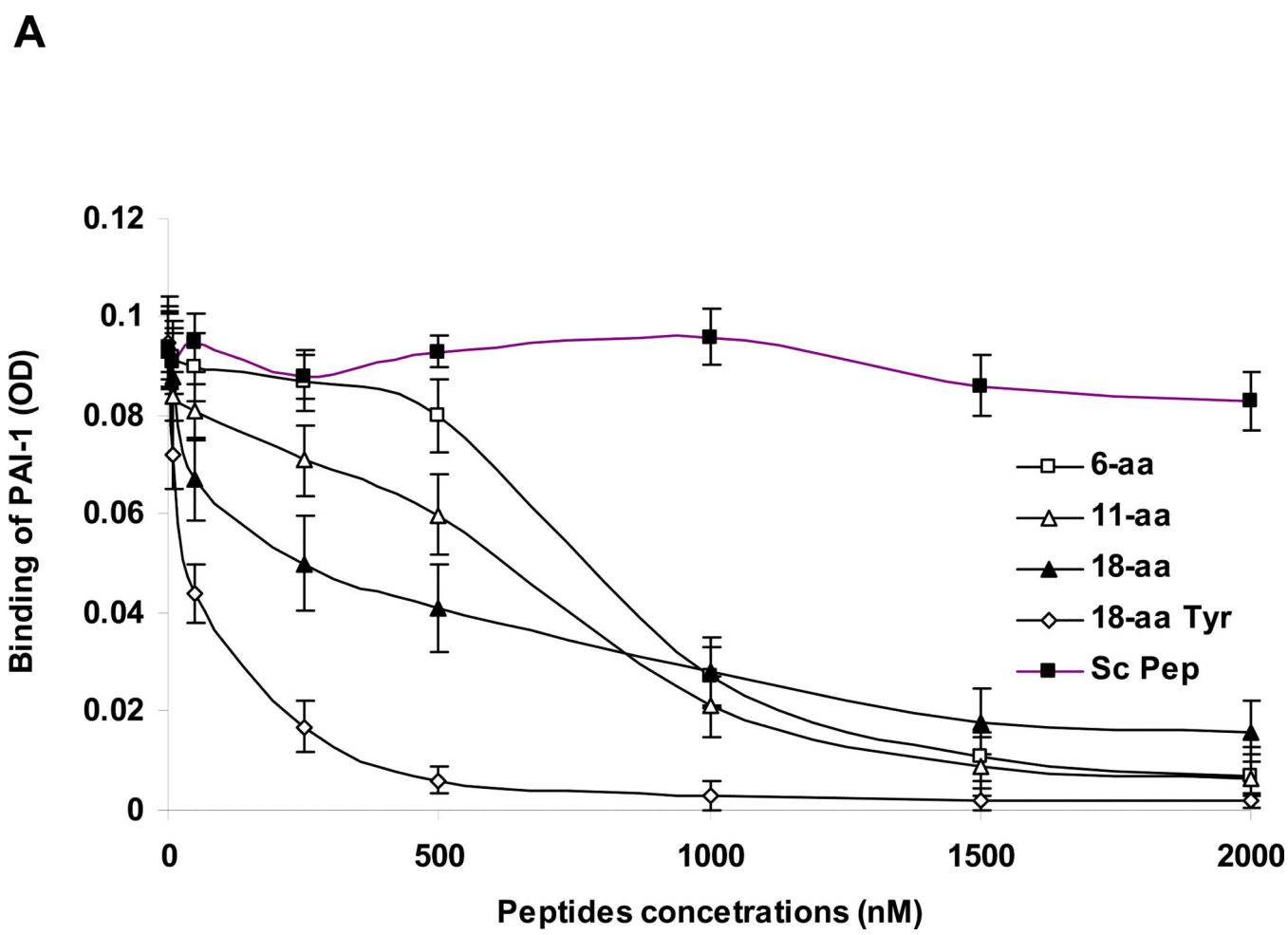

B

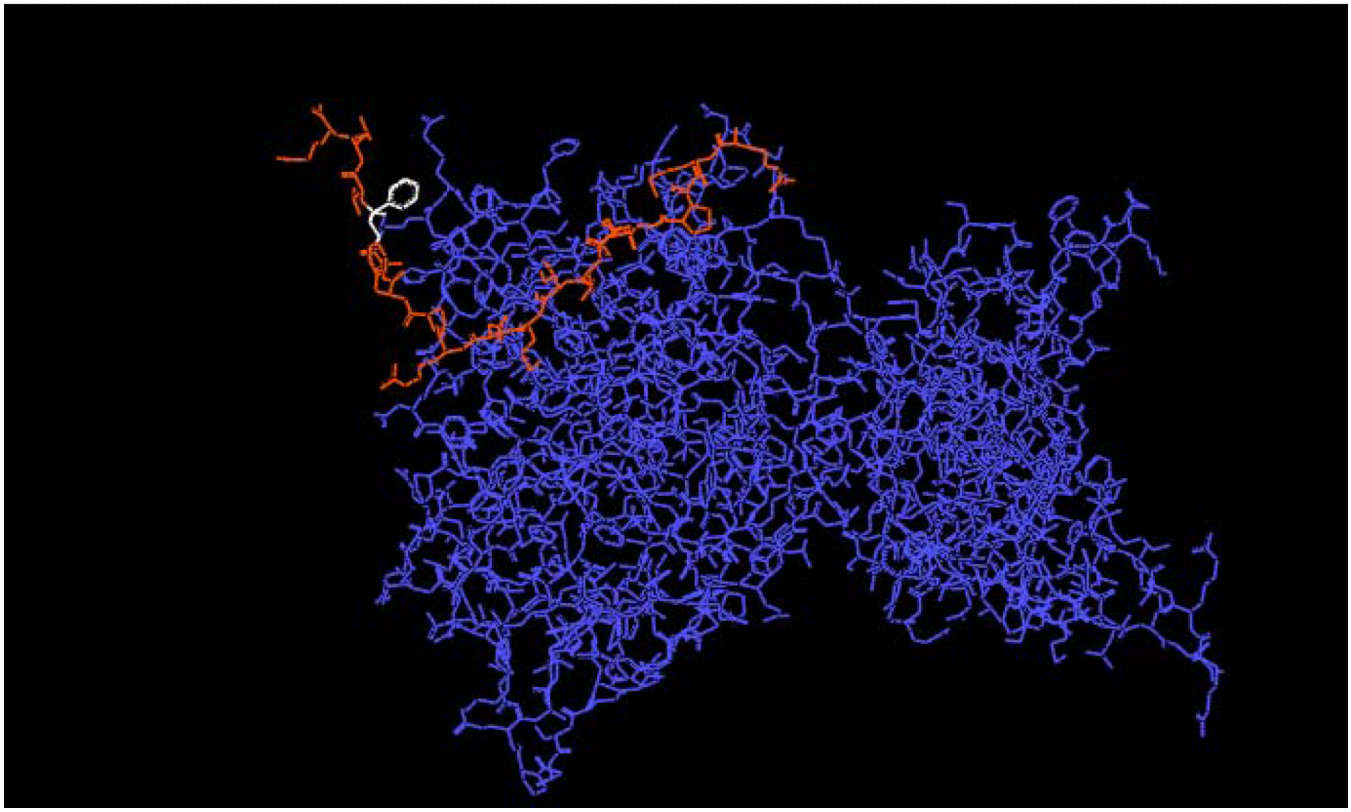

Figure 4. Panel A: Inhibition of the binding of PAI-1 to rtPA by PAI-1–derived peptides

The binding of PAI-1 (1 nM) to immobilized rtPA was measured in the absence (cont.) or presence of increasing concentrations of each of the 3 PAI-1 derived peptides. Equimolar concentrations of rtPA (tPA) served as the positive control to determine 100% inhibition. One of 3 such experiments with equivalent results is shown. **Panel B.** Energetically favorable conformation of the complex between rtPA (in blue) and the 18-aa peptide (in red) showing that the aromatic rings of Phe^{383} (in white) are directed outward toward the solvent.

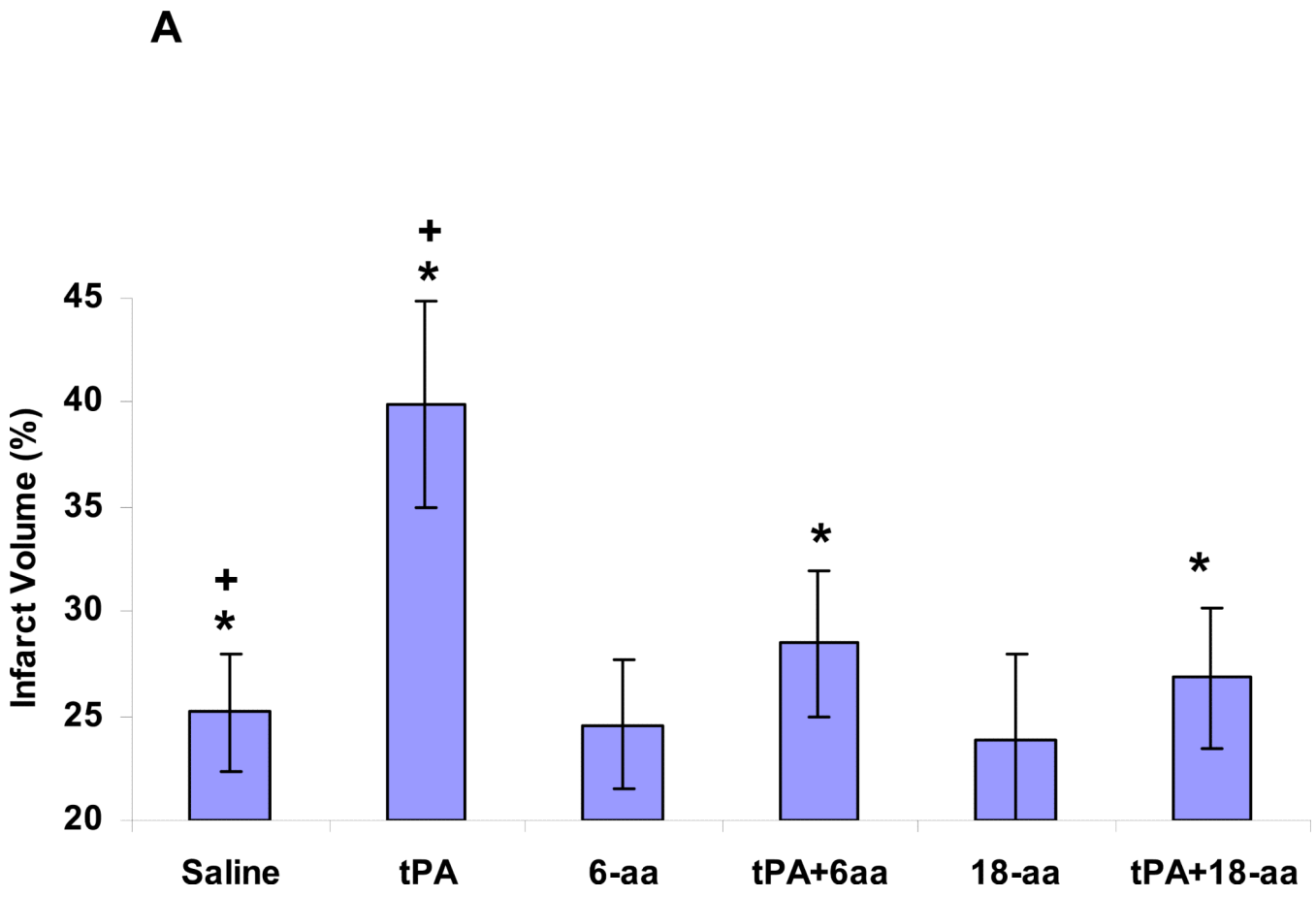

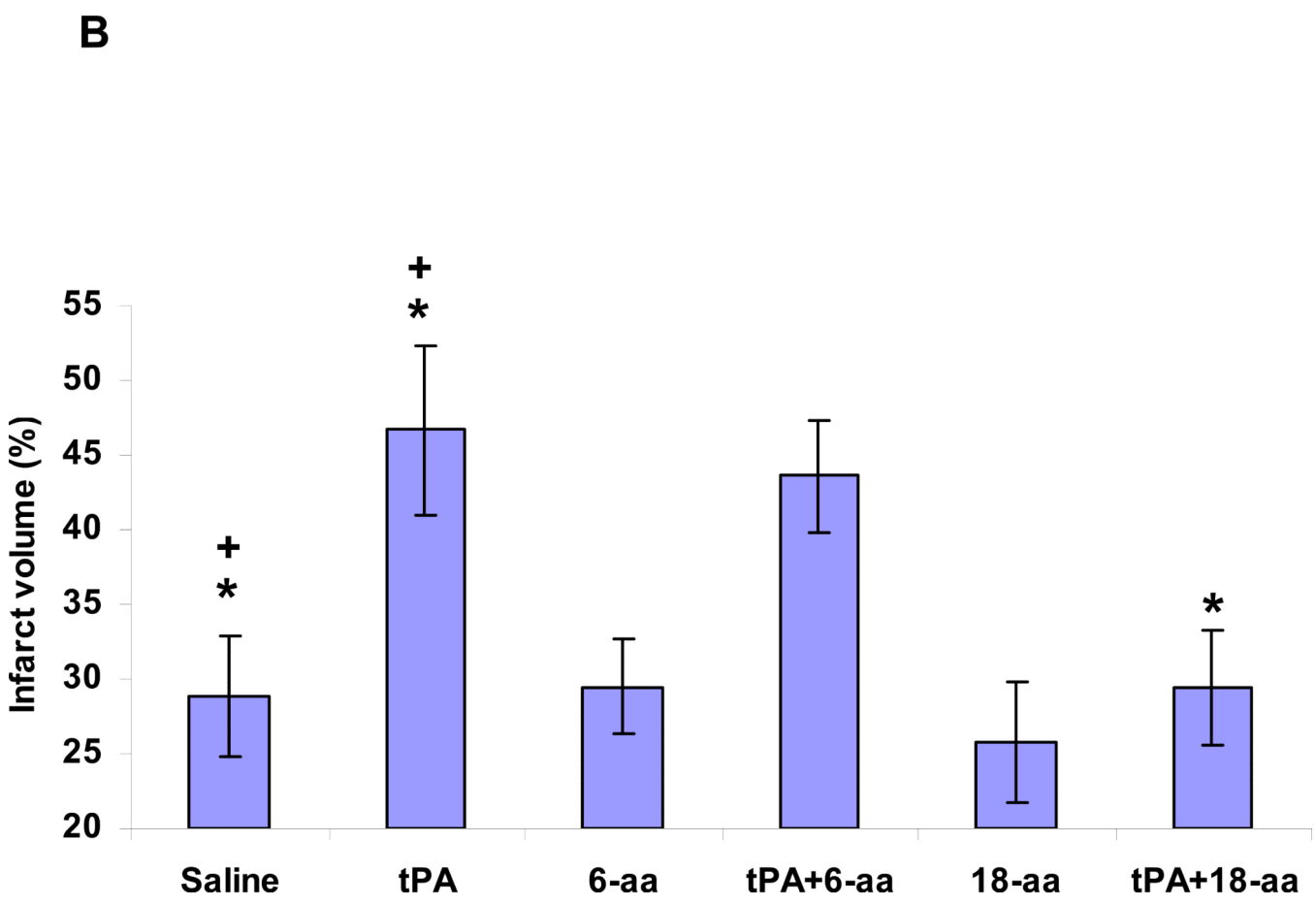

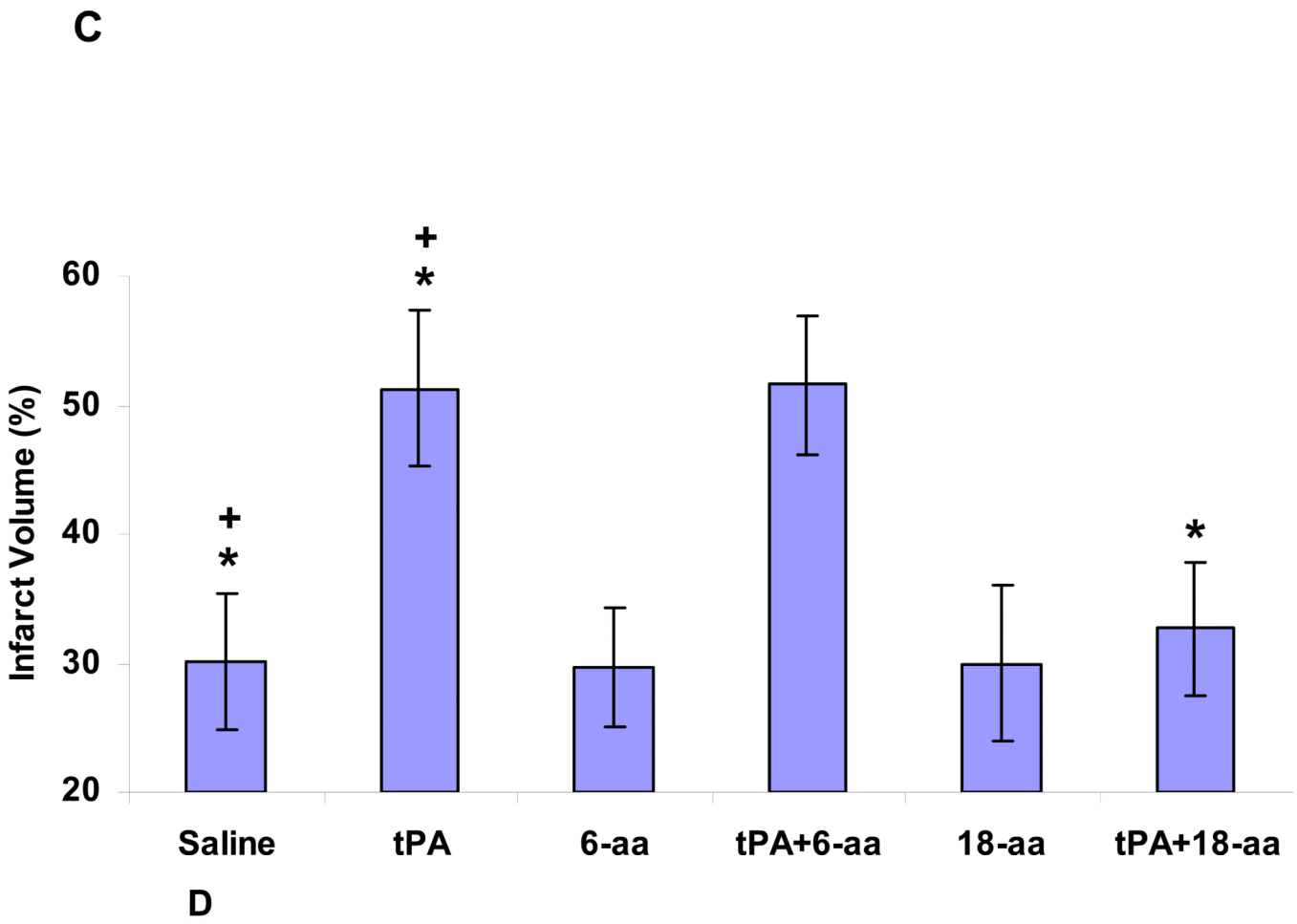

D

Figure 5. Inhibition of post ischemic rtPA-induced brain damage by PA-1 derived peptides

The MCA of rats was occluded with an intraluminal filament as described in Methods. The thread was withdrawn 1 hour later. One **(Panel 5A)**, two **(Panel 5B)** or three **(Panel 5C)** hours after withdrawal of the thread, rtPA (6 mg/kg) alone or together with the PAI-1 derived peptides 6-aa or 18-aaTyr was injected IV (1mg/kg each). Controls were injected with saline. Twenty-four hours later, brain infarct size and volumes were measured, as described in Methods. The mean ± SEM of data from 15 animals/group is shown. The appearance of representative sections is shown in **Panel 5D**.

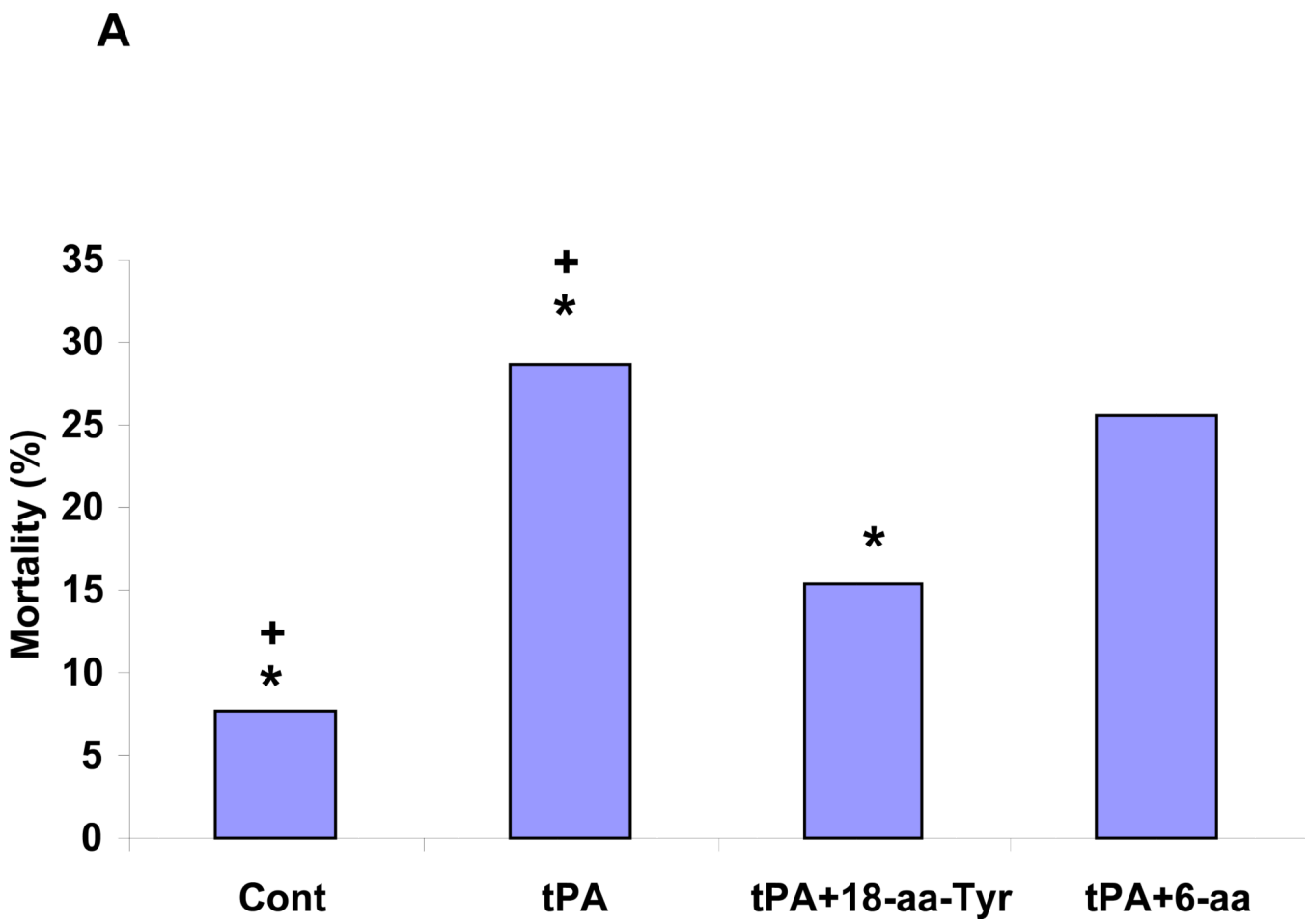

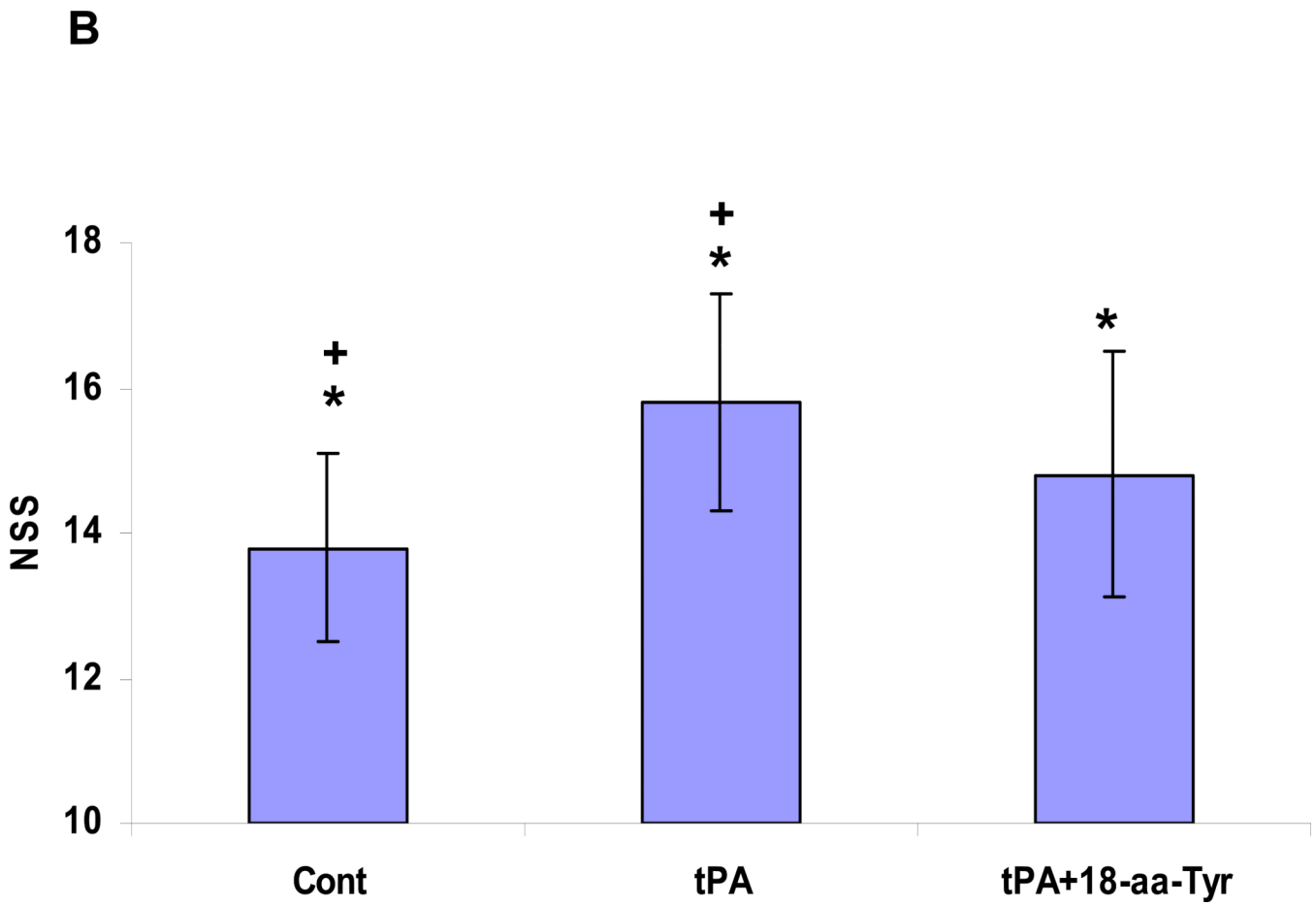

Figure 6. Effect of PAI-derived peptides on mortality and neurological recovery. Panel A. Inhibition of post ischemia rtPA-induced mortality

Animals were treated as described in the legend to Figure 5. Death was recorded. Animals were included in the study if they survived up to the initiation of treatment with saline (Cont) or with rtPA or rtPA together with the 6- or 18-aa-Tyr PAI-1 derived peptides. The number of deaths in each group was recorded. The mean from 16 animals/group is shown.

Panel B: Preservation of neurological function. Animals were treated as described in the legend to Figure 5. The neurological score was measured 24 hours after induction of ischemia in animals treated with saline (Cont), rtPA or rtPA together with 18-aa-Tyr, as described in Methods. The mean ± SEM of data from 12 animals/group is shown.

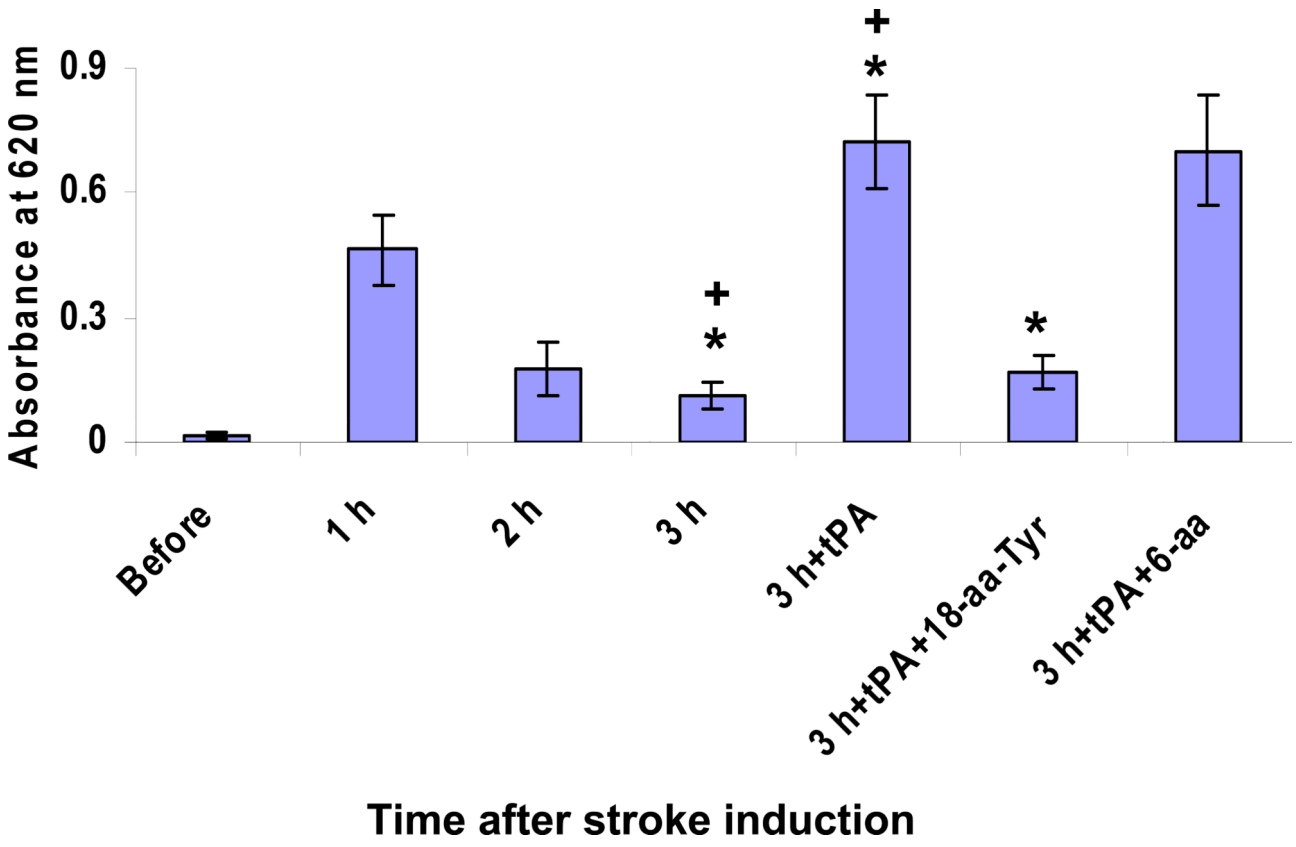

Figure 7. Time course of BBB permeability post ischemia

BBB permeability was measured in untreated animals using Evans blue as described in the legend to Figure 1, before and 1, 2 and 3 hours after induction of brain ischemia by mechanical occlusion. In second set of animals, three hours after induction of brain ischemia, BBB permeability was measured after rtPA was given alone or together with the 6- or 18-aa-Tyr PAI-1 derived peptides. The mean ± SEM of data from 12 animals/group is shown.

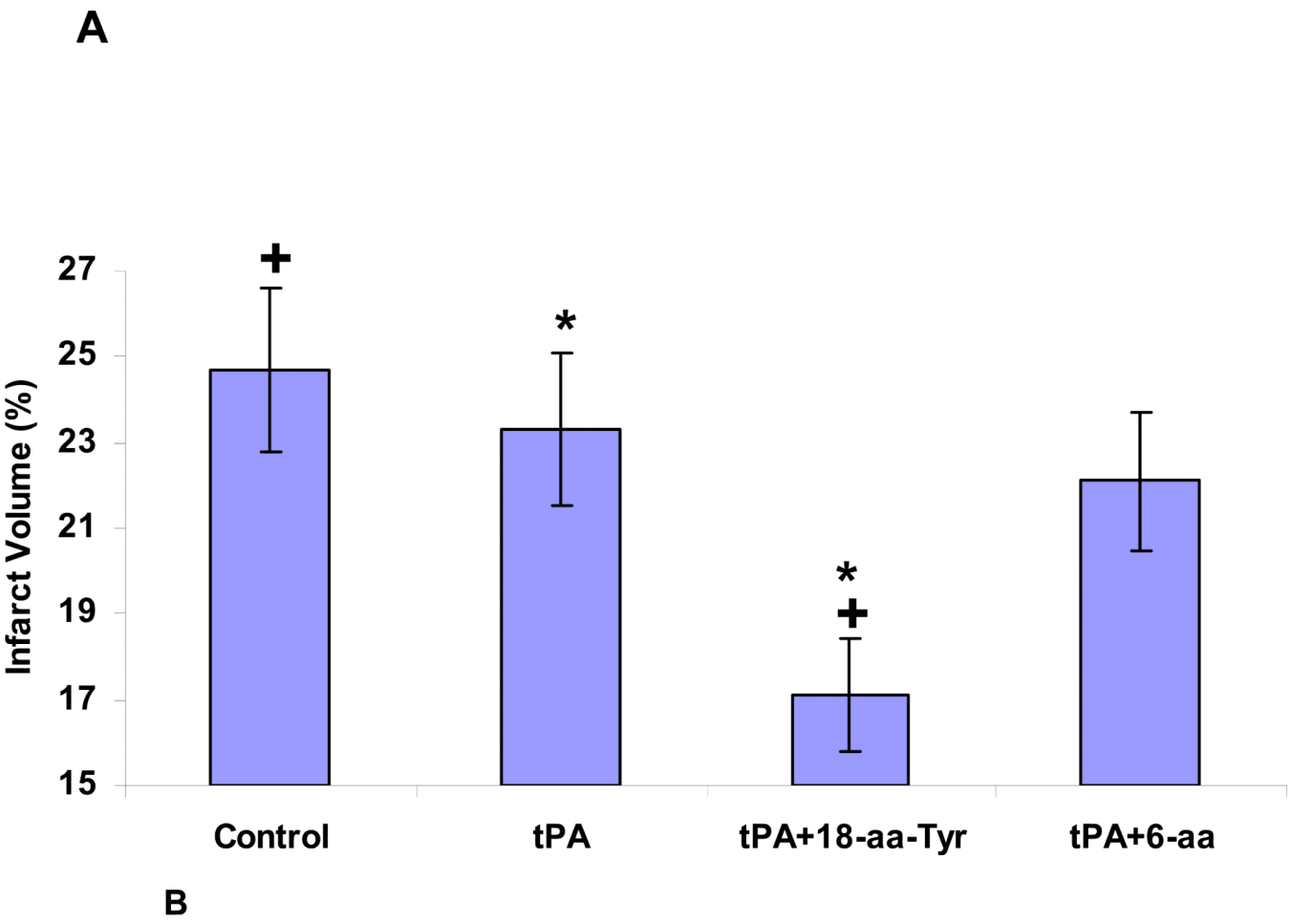

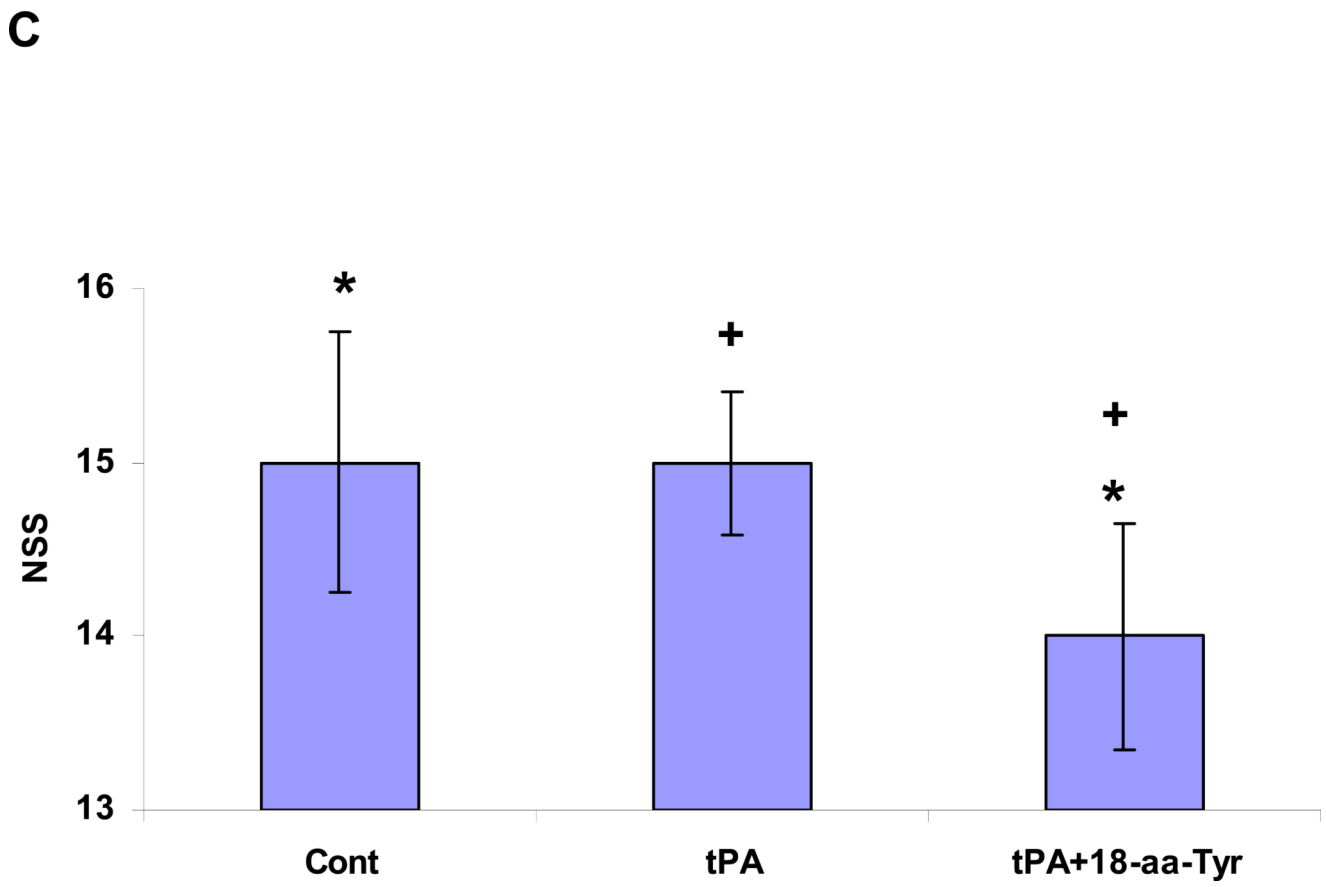

Figure 8. Neurological outcome four hours after thromboembolic stroke in rats treated with rtPA and PAI-1 derived peptides

Four hours after induction of thromboembolic stroke, rats were given saline (Cont), rtPA (6 mg/kg) alone or together with 18-aa-Tyr or 6-aa PAI-1 derive peptides (1 mg/kg each). Twenty four hours later, infarct volume **(Panels 8A and 8B)** and assessment of neurological function, expressed as the NSS **(Panel 8C)** were determined as described in Methods. The mean ± SEM of data from 12 animals/group is shown.